Reference-free damage detection, localization, and quantification in composites

Hyung Jin Lim, Hoon Sohn,[a] Chul Min Yeum, and Ji Min Kim
Department of Civil and Environmental Engineering, Korea Advanced Institute of Science and Technology, 291 Daehak-Ro, Daejeon, 305-701, South Korea

(Received 7 August 2012; revised 29 January 2013; accepted 1 April 2013)

In this study, a reference-free damage characterization technique is developed not only to identify but also to locate and quantify damage in composite structures subject to varying temperature conditions. First, damage is characterized in terms of a damage index (m-value) defined as the ratio of damage size to the wavelength of the A_0 mode within the damage. Then, a feasible solution space defining all possible combinations of the damage location and size are estimated without using any prior baseline data obtained from the pristine condition of a structure or different paths. When additional information such as the A_0 mode group velocity within the pristine region of the structure becomes available, the estimates for the damage location and size are updated with better accuracy. The uniqueness of this study lies in that damage localization and quantification as well as identification are all performed without comparing current Lamb wave signals with the ones obtained from the pristine condition of the target structure, making the proposed technique more attractive for online monitoring. Numerical and experimental tests are presented to demonstrate the effectiveness of the proposed damage detection technique under varying temperature.
 [http://dx.doi.org/10.1121/1.4802744]

PACS number(s): 43.35.Cg, 43.35.Zc [TK] Pages: 3838–3845

I. INTRODUCTION

These days, composite materials are widely accepted for a variety of applications due to their unique characteristics such as being light weight and high strength. However, temperature, humidity, impacts, and repeated cyclic stress can compromise the integrity of composite materials. In particular, impact events can seed damage, which is typically a collective outcome of delamination, fiber and matrix breakage, in composites. The main issue with the impact-induced damage is that it is often invisible from exterior surfaces although it can significantly degrade the performance of composite materials.

Lamb waves measurement has been identified as one of the promising structural health monitoring (SHM) techniques for detecting hidden damage in composites because of its long inspection range and high sensitivity.[1,2] Since early 1990s, the interactions of Lamb waves with damage in composites have been investigated by many researchers.[3,4] Then, so called damage-sensitive features are extracted based on reflection,[5–9] time delay,[10] attenuation,[11] mode conversion[12,13] and standing waves[14,15] resulted from the formation of damage.

One major issue with these features is that they are also frequently influenced by other ambient variations of the system being monitored such as temperature and loading. To minimize false alarms due to these ambient variations, advanced damage diagnoses are proposed using optimal baseline subtraction and stretch methods,[16,17] data normalization,[18,19] and reference-free and instantaneous baseline techniques.[20–22] The combined optimal baseline subtraction and stretch method compensates the effect of temperature from an initial baseline signal and subtracts the modified baseline signal from a test signal to isolate only damage relevant components. However, for the success of the combined optimal baseline subtraction and stretch method, a large volume of baseline data needs to be measured under a wide range of temperature conditions. Similarly, data normalization techniques require multiple baseline data, and damage is detected by identifying a new dataset that significantly deviates from the pool of baseline datasets. Reference-free and instantaneous baseline techniques ascertain the existence of damage either without using any baseline data or using simultaneously obtained data within the same sensor network as the reference. However, the existing reference-free and instantaneous baseline techniques are able to address only the existence of damage but not localization or quantification.

This study is a further advancement of the previous reference-free diagnosis techniques. The current study is unique in a sense that not only the existence of damage but also the location and size of damage are estimated using only the current signals obtained from a single wave propagation path but without relying on any prior baseline data or additional signals acquired from different paths. Numerical simulations and experimental tests are conducted to validate the effectiveness of the proposed technique. Artificial damage with inserted Teflon tapes and actual impact-induced damage are detected using the proposed technique, and additional tests under varying temperature conditions are performed to highlight the advantage of the proposed reference-free technique. The location and size of damage are confirmed by independent thermography and C-scan.

[a]Author to whom correspondence should be addressed. Electronic mail: hoonsohn@kaist.ac.kr

This paper is organized as follows. In Sec. II, the interaction of Lamb waves with damage in composites is briefly reviewed. Section III describes the development of the proposed damage diagnosis technique. Then, numerical simulations and experiments are reported in Secs. IV and V, respectively. Finally, the conclusion and discussions are provided in Sec. VI.

II. INTERACTION OF LAMB WAVES WITH DAMAGE IN COMPOSITES

A. The effects of damage and temperature on Lamb waves

Lamb waves are one type of guided wave that propagates in plate-like structures, and their wavelengths are in the same order of magnitude as the thickness of the structures. Vibration patterns through the thickness of a plate are quite distinctive for different types of Lamb modes (S and A modes), and the pattern even for the same mode type varies over the excitation frequency due to its dispersive characteristic.[4] In general, Lamb wave signals are collected in two different schemes: (1) pitch-catch and (2) pulse-echo schemes. In the pitch-catch scheme, a transducer mounted at one position of the structure is used for Lamb wave excitation, and the second transducer is placed at another position for sensing. In the pulse-echo scheme, only one transducer is used and acts as both an actuator and a sensor.

The A_0 Lamb wave mode (A_0 mode) is used for delamination diagnosis in this study because the A_0 mode is sensitive to subsurface defects due to its out-of-plane wave motion.[8–10] Although there are other converted modes produced by the delamination, it is confirmed that the A_0 mode is the dominant mode reflected from the delamination.[7–10] Furthermore, the amplitudes of the other converted modes are not only at least 1 order of magnitude smaller than that of the A_0 mode but also much smaller than the mode decomposition error. Therefore, their effects are ignored in this study.

Figure 1 is presented to justify the development of the proposed reference-free damage diagnosis technique. In Fig. 1(a), the time delay and amplitude decrease of the A_0 mode due to damage formation are shown for the pitch-catch signals obtained from a specimen with and without an impact-induced damage. The detailed description of the experiment data presented in this figure is provided in Sec. V. In Fig. 1(a), the reduction of the effective thickness within the damage area causes the change of the A_0 mode group velocity and consequently the time delay of the A_0 mode.[7] In addition, the shear modulus reduction within the damage area produces the scattering of the incident waves at the boundary of the damage when the A_0 mode is propagating through the damage area. By taking advantage of the time delay and attenuation of Lamb waves, a large volume of damage detection techniques has been developed.[10,11] One problem with these existing techniques is that simple temperature variation can also produce similar time delay and attenuation effects as shown in Fig. 1(b). Therefore, conventional damage detection techniques based on comparison with baseline signals can suffer from false alarms when the system is exposed to real operational conditions such as temperature variation.

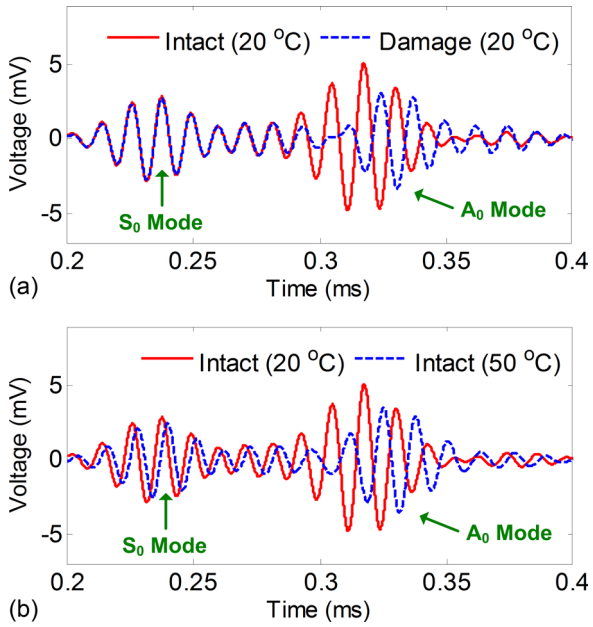

FIG. 1. (Color online) (a) Time delay and attenuation of the A_0 mode due to an impact-induced damage (impact 3). (b) Temperature variation observed in the pitch-catch Lamb wave signals measured from a composite plate specimen without the damage.

B. Multiple reflections within damage

Besides the time delay and attenuation, it has been reported that multiple reflections occur within the damage area as shown in Fig. 2. When a propagating A_0 mode enters a damage area, a portion of the wave passes through the damage area (the transmitted A_0 mode: $A_{0,T}$) and the rest travels through the damage after reflected at the entering and exiting boundaries of the damage several times. Subsequently, the reflected waves trapped inside the damage produce standing waves confirmed by numerical simulations and ultrasonic wave field imaging techniques using a scanning laser vibrometer.[14,15] In this study, the first A_0 mode wave packet reflected from the inside of damage (the first reflected A_0 mode: $A_{0,R}$) is used as a damage-sensitive feature.

C. Damage index (*m*-value)

The time difference (Δt) between $A_{0,T}$ and $A_{0,R}$ arrivals depends on the physical damage length (d) and the A_0 mode group velocity within the damage area (ν_d). Here, the A_0 mode group velocity is a function of the shear modulus (G)

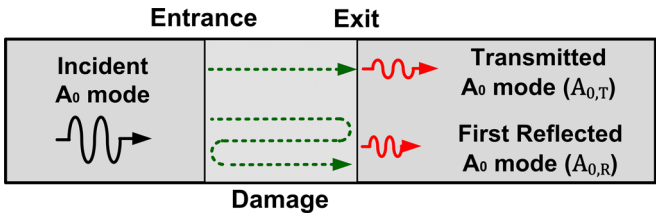

FIG. 2. (Color online) Multiple A_0 mode reflections within the damage area. When a propagating A_0 mode enters a damage area, a portion of the wave directly passes through the damage area and the rest travels through the damage after reflected at the entering and exiting boundaries of the damage several times. In this study, the A_0 mode wave packet first reflected from the inside of damage ($A_{0,R}$) is used for damage diagnosis.

within the waveguide, and Δt is related to d and ν_d as follows:

$$\Delta t = \frac{2d}{\nu_d}. \tag{1}$$

The objective here is to estimate d and ν_d from the measured arrival time difference, Δt. However, Eq. (1) and finite element (FE) simulation in Fig. 3 show that d and ν_d values cannot be uniquely determined from Δt. Figure 3(a) represents two FE models with the same Δt but with different d and ν_d values, and Fig. 3(b) shows the A_0 mode signals obtained from these two models. To address this issue, a damage index (m-value) is defined as follows:

$$m = \frac{d}{\lambda_d} = \frac{\xi \Delta t}{2}, \tag{2}$$

where ξ is the central frequency of the A_0 mode, and λ_d is the wavelength of the A_0 mode within the damage area. Detailed descriptions of the FE model are presented in Sec. IV. Here, the m-value represents all possible combinations of d and ν_d that can reproduce the measured signal when the A_0 mode group velocity (ν_i) within the pristine region of the structure at ξ is unknown. That is, the m-value acts as a damage indicator when ν_i is unknown. Once ν_i is either measured or estimated, d and ν_d can be calculated uniquely. However, it should be noted that ν_i is often unknown and varies even when it is known because of changing temperature conditions of the target structure.

In practice, Δt cannot be easily computed because $A_{0,T}$ and $A_{0,R}$ mode wave packets often overlap each other. In this study, a matching pursuit method[23,24] is used to extract $A_{0,T}$ and $A_{0,R}$ mode wave packets and estimate their arrival times. The details on the matching pursuit method are described in Sec. III.

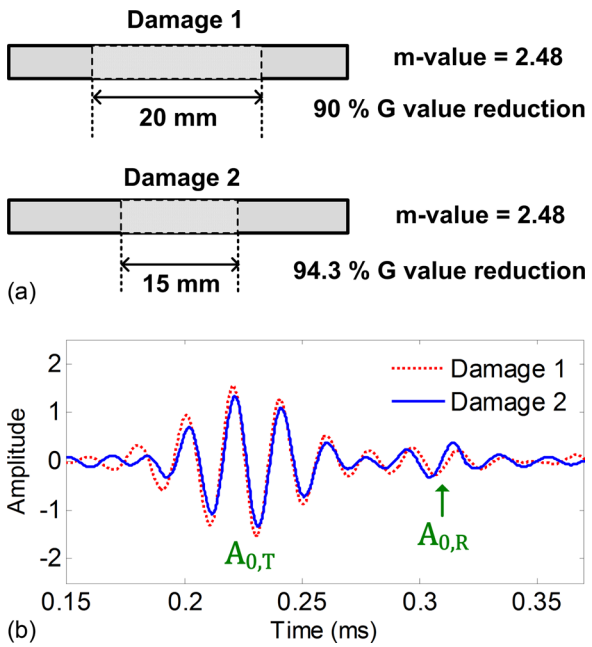

FIG. 3. (Color online) (a) Two FE models which have the same m-value defined in Eq. (2) but different damage lengths and reduced shear modulus values (G) within the damage areas. (b) A_0 mode signals obtained from the above two different FE models with the same m-value.

III. THEORETICAL DEVELOPMENT

A. Notations and overview

Figure 4 presents variables used in the proposed damage characterization technique. ν_i is the A_0 mode group velocity within the pristine region of structure at a specific excitation frequency. t_d is the travel time of the A_0 mode from the entrance to the exit of the damage. Note that t_d is half of Δt defined in Eq. (1). d is the distance between the entrance and the exit of the damage and is referred to as a physical damage length in this paper. l_1 is the distance from the excitation PZT (PZT A) to the entrance of the damage, and l_2 is the distance from the sensing PZT (PZT B) to the exit of damage. t_1 and t_2 are the travel times of the A_0 mode within l_1 and l_2, respectively. Finally, the distance and travel time (arrival time) of the A_0 mode from PZT A to PZT B are computed as follows:

$$l = l_1 + d + l_2, \quad t = t_1 + t_d + t_2. \tag{3}$$

The overall process of the proposed damage characterization technique can be summarized as follows: (1) Identify the damage existence by detecting the appearance of the $A_{0,R}$ mode wave packet from damage, (2) compute Δt, which is the arrival time difference between the $A_{0,T}$ and $A_{0,R}$ modes, and (3) estimate the damage index (m-value), the damage length (d) and the damage location (l_1). Note that only t and t_d are measured using the pitch-catch scheme and ν_i and ν_d are estimated from the measured t and t_d. Then, d is obtained using the relationship $d = \nu_d t_d$. Moreover, t_1 is measured with the pulse-echo scheme, and l_1 is estimated from the relationship $l_1 = \nu_i t_1$. The detailed theoretical formulation is presented below.

B. A_0 mode decomposition and extraction of transmitted and reflected A_0 modes

The first step in the proposed technique is to decompose only A_0 modes from measured Lamb wave signals. This decomposition is achieved using the mode decomposition technique developed by the authors' group.[25] The uniqueness of the decomposition technique is to use a pair of dual PZTs, which are composed of concentric ring and circular segments.

A particular response signal, $V(t)$, obtained by a pair of dual PZTs can be divided into two components: (1) the normalized time responses for S_0 and A_0 modes, $C^{S_0}(t,l)$ and

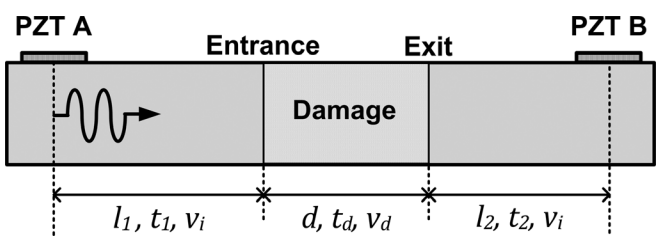

FIG. 4. Variables used in the proposed damage characterization technique.

$C^{A_0}(t,l)$, controlled by the distance between the excitation and sensing PZTs, l, and (2) the scaling factors, $S^{S_0}(a,c)$ and $S^{A_0}(a,c)$, controlled by the sizes of the excitation and sensing PZTs, a and c,

$$V(t) = C^{S_0}(t,l)S^{S_0}(a,c) + C^{A_0}(t,l)S^{A_0}(a,c). \quad (4)$$

By independently or simultaneously activating different parts of the excitation and sensing dual PZTs, multiple Lamb wave signals with different excitation and sensing PZT sizes can be obtained from a pair of dual PZT transducers. Then, the normalized time responses, $C^{S_0}(t,l)$ and $C^{A_0}(t,l)$, can be obtained from the multiple Lamb wave signals. Further details are provided in Yeum *et al.*[25]

Once the normalized A_0 mode signal is decomposed from the measured Lamb wave signals, individual A_0 mode wave packets such as $A_{0,T}$ and $A_{0,R}$ can be extracted by the matching pursuit method[23,24] and the normalized A_0 mode signal can be represented as a linear combination of these wave packets. In this study, only $A_{0,T}$ and $A_{0,R}$ mode wave packets are extracted, ignoring additional reflected wave packets from the boundaries of structure. That is, only the amplitude, arrival time, scale (width), central frequency and phase of the $A_{0,T}$ and $A_{0,R}$ mode wave packets are estimated from the normalized A_0 mode signal. Note that the application of the matching pursuit method becomes particularly important when t_d and t_1 need to be estimated from overlapping $A_{0,T}$ and $A_{0,R}$ mode wave packets.

C. Damage detection, localization, and quantification

1. Damage identification

As each wave packet passes through the damage area and travels a longer distance, its scale (width) increases due to the dispersive nature of Lamb waves. Based on this observation, the existence of damage is identified when the scale of the $A_{0,R}$ mode wave packet becomes wider than that of $A_{0,T}$.

2. Level 1

Once t and t_d are estimated using the matching pursue method, it can be easily shown from Fig. 4 that ν_i and ν_d are simply linear functions of d for the fixed t and t_d values,

$$\nu_i = \frac{l-d}{t-t_d} \quad \text{and} \quad \nu_d = \frac{d}{t_d} = \frac{\xi}{m}d, \quad (5)$$

ν_i and ν_d values in Eq. (5) are shown as linear functions of d in Fig. 5. By comparing Eq. (2) and the second term of Eq. (5), it can be easily seen that the slope of the linear function for $\nu_d(=\xi d/m)$ indeed reveals the m-value. Furthermore, because $0<d<l$ and $\nu_i > \nu_d$, the feasible ranges for ν_i and ν_d can be specified as follows:

$$\frac{l}{t} < \nu_i < \frac{l}{t-t_d} \quad \text{and} \quad 0 < \nu_d < \frac{l}{t}. \quad (6)$$

The ν_i and ν_d lines in Fig. 5(a) represent all feasible combinations of ν_i, ν_d, and d given t and t_d values. In other words, the feasible solution ranges of ν_i, ν_d, and d are estimated sorely based on the measurement of t and t_d.

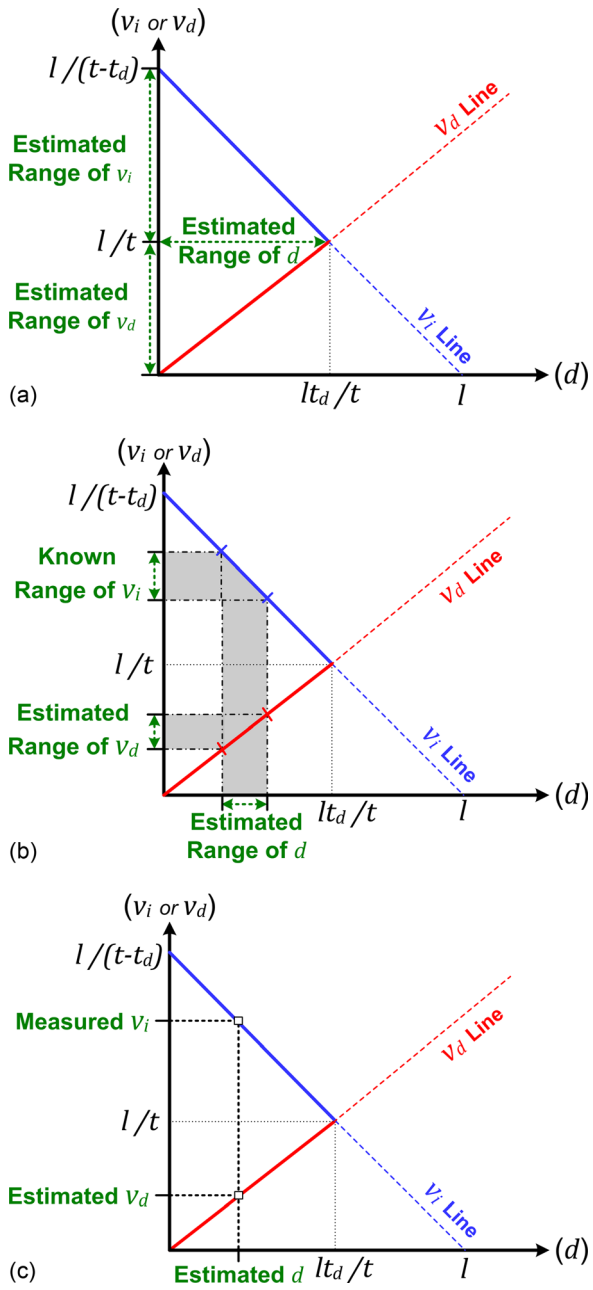

FIG. 5. (Color online) Different levels of damage quantification and localization: possible solution spaces for ν_i, ν_d, and d. (a) Level 1: Estimation of the possible ranges of ν_i, ν_d, and d values sorely based on the measurement of t and t_d. (b) Level 2: Estimation of ν_d and d ranges with an known range of ν_i and the measurement of t and t_d. (c) Level 3: Estimation of unique ν_d and d values with the measurement of ν_i, t, and t_d.

3. Level 2

When the value of ν_i can be limited to a certain range, more precise estimates of ν_d and d become possible. For instance, when the range of ν_i is known or can be estimated under changing temperature conditions, the ranges of ν_d and d can be better confined as shown in Fig. 5(b).

4. Level 3

When ν_i is known in advance or estimated from a nearby reference path in a sensor network, ν_d and d values can be uniquely determined as shown in Fig. 5(c). Note that by measuring t_1 from the pulse-echo scheme, the solution

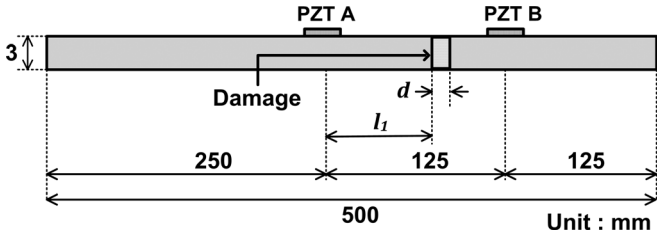

FIG. 6. An FE model used for verification of the proposed damage characterization technique.

space for the possible combinations of l_1 and d can be also obtained in a similar manners, allowing damage localization based on the estimated l_1.

IV. NUMERICAL SIMULATION

The feasibility of the proposed damage characterization technique is first verified by 2-D FE simulation using MSC. PATRAN and NASTRAN. Figure 6 presents the FE model, a pair of dual PZTs and damage, respectively. The driving frequency was selected to be 50 kHz so that only fundamental Lamb wave modes (S_0 and A_0 modes) were generated, and 0.5 mm × 0.5 mm square shell elements were used considering the wavelength of the A_0 mode. The sampling rate was set to 5 Ms/s and the Rayleigh damping coefficients were set to 10^{-4} for a mass damping and 0 for a stiffness damping, respectably.

The PZTs were assumed to be perfectly bonded to the structure and have no mechanical loss. The input force exerted by the excitation PZT (PZT A) was modeled as "pin-forces" applied along equally spaced points of its boundary. The corresponding response at the sensing PZT (PZT B) was computed by modeling PZT B with multiple meshes and integrating the strain over the entire PZT area.

The composite plate was assumed to have the isotropic material properties only along the wave propagation direction.

TABLE I. Material properties of the FE model and the test specimens.

Property	Value
Tensile Modulus (E)	59 Gpa
Shear Modulus (G)	24 Gpa
Specific Gravity	1.6

The effective material properties of the test specimens presented in Sec. V were experimentally measured and provided by the composite manufacturing company (Nexcoms Inc.), and the same material properties were used for the FE model as shown in Table I. Note that the material properties of the composite is assumed to be constant only along each path, and the directionality of the wave velocity is considered in the proposed technique. With a network of PZT transducers, the damage area can be approximated from the damage lengths estimated from each of the multiple wave propagation paths.

Impact-induced damage was modeled by reducing the shear modulus (G) within the damage area.[26–29] The damage location, the physical damage length and the percentage of the shear modulus reduction are presented in Table II. Table II also presents the results of the proposed damage characterization. For all three cases, it is shown that the exact ν_i, ν_d, and d values fall within the ranges of ν_i, ν_d, and d ranges estimated by Level 1. When the variation of ν_i is limited to ±5% (1190–1316 m/s) of the measured ν_i (1253 m/s) in Level 2, the ranges of the possible solution spaces are better confined. Finally, when ν_i is known, the estimated ν_i, ν_d, and d values converge to the exact values (Level 3).

V. EXPERIMENTAL VERIFICATION

A. Experimental setup

Two carbon composite plates with a dimension of 500 mm × 500 mm × 3 mm were manufactured by stacking 12 layers of woven fabrics type prepregs. The effective

TABLE II. Damage characterization results (Simulation).

Damage Conditions		m	l_1 (mm)	d (mm)	ν_d (m/s)
Case 1 (90% **G** reduction)	Exact	2.56	65.0	20.0	390
	Level 1	2.48	47.2 – 74.7	0.0 – 46.1	0 – 930
	Level 2[a]	2.48	60.3 – 66.7	13.5 – 24.1	271 – 486
	Level 3[b]	2.48	63.5	18.8	379
Case 2 (90% **G** reduction)	Exact	1.82	67.5	15.0	410
	Level 1	1.93	51.9 – 75.1	0.0 – 38.6	0 – 1000
	Level 2[a]	1.93	61.8 – 68.2	11.4 – 22.2	295 – 575
	Level 3[b]	1.93	65	16.8	435
Case 3 (93% **G** reduction)	Exact	2.40	67.5	15.0	312
	Level 1	2.33	51.8 – 79.1	0.0 – 43.1	0 – 924
	Level 2[a]	2.33	66.8 – 73.8	8.5 – 19.6	182 – 419
	Level 3[b]	2.33	70.3	14.0	301
Case 4 (90% **G** reduction)	Exact	1.97	90.0	15.0	380
	Level 1	1.95	71.1 – 102.7	0.0 – 38.4	0 – 984
	Level 2[a]	1.95	86.0 – 95.1	10.7 – 21.6	264 – 530
	Level 3[b]	1.95	90.6	16.2	397

[a]The variation of ν_i was assumed to ±5% of the measured ν_i (1190 – 1316 m/s).
[b]Measured ν_i: 1253 m/s.

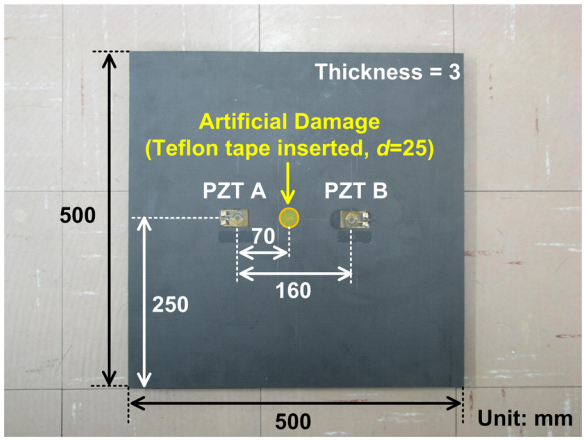

FIG. 7. (Color online) A composite specimen with artificially inserted-Teflon tapes. An additional identical specimen with an impact-induced damage was also tested but not shown here.

material properties of the specimens are presented in Table I. In one of the specimens, 25 mm diameter Teflon tapes were inserted at the center of the specimen in every 3 layers to mimic delamination. Real impact damage was introduced to the other specimen by dropping a 5 kg mass with a 10 mm round tip from 0.15 m height three times. The Lamb wave signals were measured after each impact.

Two identical dual PZTs were installed on each specimen as shown in Fig. 7. Each dual PZT consists of a circular segment with 8 mm diameter and a ring segment with 9 mm and 18 mm inner and outer diameters, respectively. A detail description of the dual PZT is presented in Yeum *et al.*[25]

The data acquisition system (NI PXI) consists of an arbitrary waveform generator (AWG, NI PXI-5421), a high speed signal digitizer (DIG, NI PXI-5122) and two multiplexers (MUX, NI PXI-2593) (Fig. 8). Using the AWG, a tone-burst input signal with a ±10 peak-to-peak voltage and 50 kHz central frequency was generated and applied. The central frequency was selected to generate only fundamental Lamb wave modes (S_0 and A_0 modes). The output voltage was measured by the DIG at a sampling rate of 5 MHz. Both pitch-catch and pulse-echo signals were measured 20 times and averaged in the time domain to improve the signal-to-noise ratio. For the pulse-echo measurement, the self-sensing circuit was installed between PZT A and the DIG.[30]

In reality, structures are subjected to changing environmental conditions such as temperature variation that can adversely affect measured signals and cause false-alarms. Thus, the robustness of the proposed damage characterization technique under varying temperature conditions was also investigated.

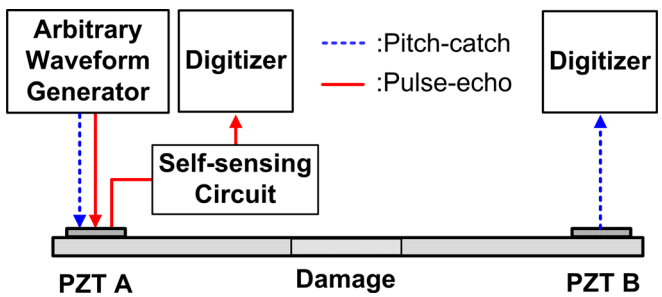

FIG. 8. (Color online) Experimental setup.

The specimens were placed inside a temperature chamber one at a time, and a thermocouple was installed on each specimen to measure its surface temperature. Lamb wave signals were obtained under three different temperature conditions (0 °C, 20 °C, and 50 °C), and the humidity was kept at 30%.

Note that l_1 and d estimated by conventional thermography and C-scan images are referred to as the exact values in Fig. 11. As one of the most widely used active thermography method, the lock-in thermography was performed[31] to confirm l_1 and d estimated by the proposed technique. The thermography image was obtained using an infrared camera (VarioCAM hr by InfraTec GmbH) and analyzed using the commercial software IRBIS. l_1 and d were estimated by measuring the number of pixels and their distance from the thermography image. Conventional C-scan image was also obtained using the water immersion type Ez-scan VII system developed by Orient NDT Inc. l_1 and d were estimated using built-in Ez-scan post processing software.

B. Teflon-inserted damage

Figure 9 shows an example of pitch-catch signals obtained from the specimen with Teflon-inserted damage obtained at 20 °C by identifying the existence of the $A_{0,R}$ mode wave packet using the matching pursuit method. This artificial damage with Teflon insertion is successfully detected by extracting the $A_{0,R}$ mode wave packet using the matching pursuit method. Similar results were obtained under the other temperature conditions as well. Table III presents the damage characterization results under temperature variation. ν_i for Level 3 was measured to be 1348 m/s at 0 °C, 1296 m/s at 20 °C and 1168 m/s at 50 °C, respectively.

The ranges of ν_i, ν_d, and d estimated by method 1 embrace all the exact values under temperature variation. Next, the limit of ν_i was assumed ±10% of measured ν_i value

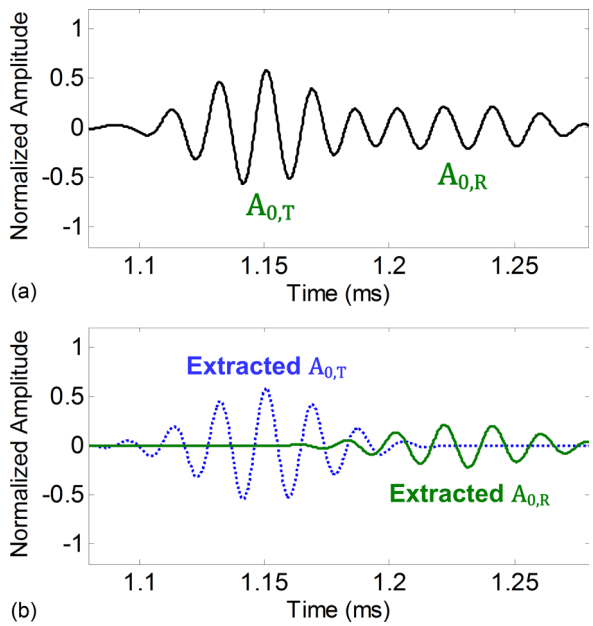

FIG. 9. (Color online) (a) The decomposition of A_0 mode signal obtained from the specimen with Teflon-inserted damage at 20 °C. (b) Damage identification by detecting the existence of $A_{0,R}$ mode wave packet using the matching pursuit method (Damage detected).

TABLE III. Damage characterization results under temperature variation (Teflon-inserted damage).

Temperature		m	l_1 (mm)	d (mm)	ν_d (m/s)
0 °C	Exact	N/A	57.7	25.0	N/A
	Level 1	1.54	52.2 – 69.0	0.0 – 37.8	0 – 1226
	Level 2[a]	1.54	52.7 – 63.8	23.7 – 27.4	770 – 890
	Level 3[b]	1.54	58.0	25.6	830
20 °C	Exact	N/A	57.7	25.0	N/A
	Level 1	1.75	53.3 – 71.3	0.0 – 40.5	0 – 1157
	Level 2[a]	1.75	53.7 – 65.6	24.7 – 27.6	706 – 780
	Level 3[b]	1.75	59.6	26.2	748
50 °C	Exact	N/A	57.7	25.0	N/A
	Level 1	1.85	51.2 – 68.0	0.0 – 39.0	0 – 1156
	Level 2[a]	1.85	51.4 – 62.6	24.1 – 28.1	652 – 761
	Level 3[b]	1.85	56.9	26.1	707

[a]The variation of ν_i was assumed to ±10% of the measured ν_i at 20 °C (1166–1425 m/s).
[b]Measured ν_i: 1348 m/s at 0 °C, 1296 m/s at 20 °C and 1168 m/s at 50 °C.

at 20 °C (1166–1425 m/s) for method 2. As we move from Level 1 to Levels 2 and 3, the estimated values of ν_i, ν_d, and d approach to the exact values even under temperature variation. Here, the comparison between the estimated and exact ν_d values is not presented because the exact ν_d is unknown.

C. Impact-induced damage

Before introducing any defect into the specimen, a damage diagnosis was performed under a pristine condition of the specimen to ensure that no false alarm was produced simply because of temperature variation. Figure 10 presents the damage diagnosis results obtained from the pristine condition of the specimen at 20 °C. No apparent $A_{0,R}$ mode wave packet was extracted indicating no sign of false alarms. Similar results were obtained from the rest of the temperature experiments although they are not reported in this paper.

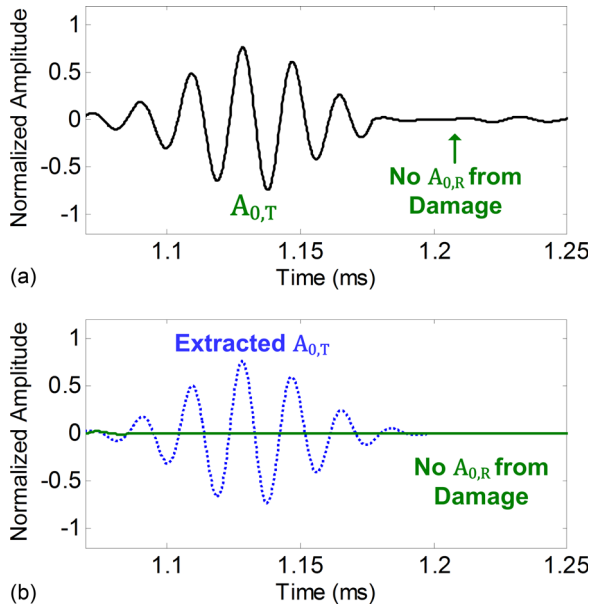

FIG. 10. (Color online) (a) Decomposition of the A_0 mode signal obtained from the pristine condition of the specimen at 20 °C. (b) Damage identification by detecting the existence of $A_{0,R}$ mode wave packet using the matching pursuit method (No damage detected).

The damage characterization results are shown on the solution space for the impact-induced damage under repeated impact tests and temperature variation in Fig. 11. The line, cross, square, and circle represent the estimated values from Levels 1, 2, 3, and the exact values, respectively. The variation of ν_i was assumed to ±10% of the measured ν_i at 20 °C (1166–1425 m/s). ν_i was measured to be 1348 m/s at 0 °C, 1296 m/s at 20 °C and 1168 m/s at 50 °C, respectively. As the number of impacts increased in Fig. 11(a) and 11(b), ν_d becomes slower after every impact although d did not grow. In Fig. 11(c) and 11(d), the damage after three impacts was characterized under temperature variations. The results show

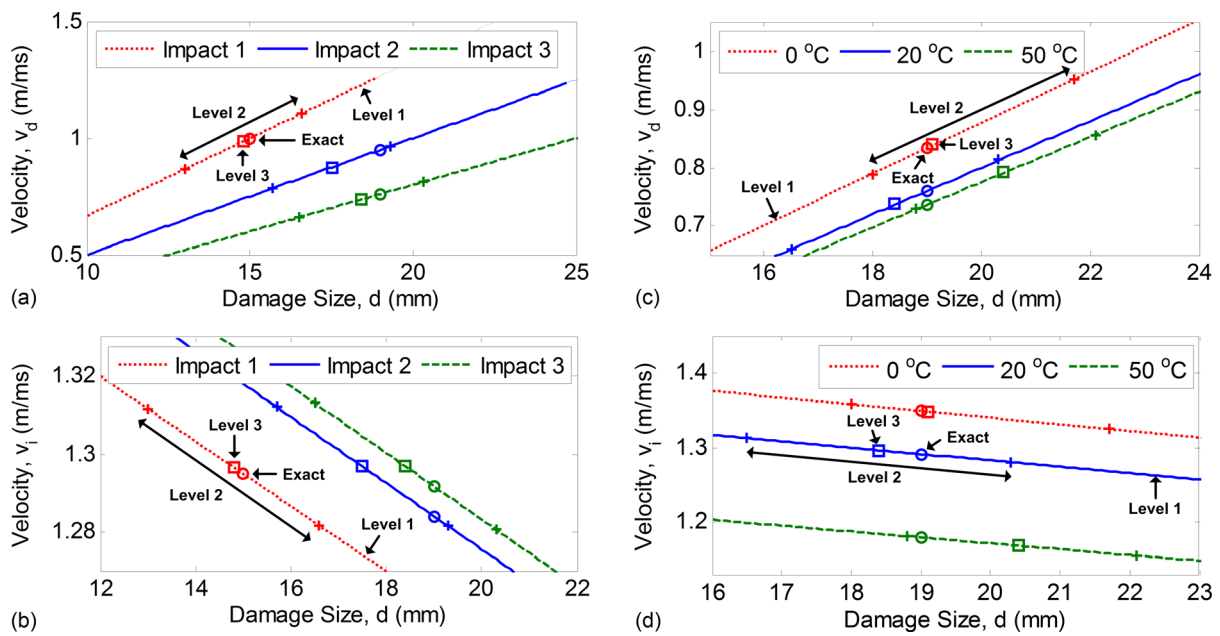

FIG. 11. (Color online) (a) ν_d and d values estimated under repeated impact tests (20 °C). (b) ν_i and d values estimated under repeated impact tests (20 °C). (c) ν_d and d values estimated after impact 3 test under temperature variation. (d) ν_i and d values estimated after impact 3 test under temperature variation.

that the impact-induced damage is successfully characterized using the proposed damage characterization technique even under temperature variations.

VI. CONCLUSION

In this study, a reference-free damage characterization technique was developed for composite plates so that the presence, location, and size of damage can be estimated solely from instantaneously obtained guided wave signals without comparison with previously obtained baseline signals. First, a damage index (*m*-value), which is defined as the ratio of a damage size to a wavelength of the A_0 mode traveling inside the damage area, was used to characterize the effective damage size. Then, a feasible solution space defining all possible combinations of the damage location and size was estimated exclusively based on the arrival time of the first A_0 mode reflected from the damage area. Finally, the estimates for the damage location and size were updated with better accuracy when additional information such as the A_0 mode group velocity within the pristine region of the structure becomes available. Numerical simulations and experimental tests were conducted to demonstrate the effectiveness of the proposed technique. The results indicated that the proposed damage characterization technique successfully estimated the location and size of Teflon-inserted and impact-induced damages even under varying temperature conditions. When a PZT sensor network is installed on a structure, other existing techniques can be first used to identify the wave propagation paths affected by a defect, and then the damage area can be approximated using the damage locations and lengths estimated by the proposed technique from each of the multiple wave propagation paths. However, because the effects of reflections from structural boundaries are ignored in this study, the applicability of the proposed technique is currently limited only to pitch-catch signals obtained away from structural boundaries of a simple composite plate.

ACKNOWLEDGMENTS

This work was supported by the Nuclear Energy Development Program (2011-0018430) and the National Research Lab (NRL) Program (2012-0005630) of National Research Foundation of Korea (NRF) funded by Ministry of Education, Science and Technology (MEST).

[1]P. Cawley and D. Alleyne, "The use of Lamb waves for the long range inspection of large structures," Ultrasonics **34**, 287–290 (1996).
[2]T. Ghosh, T. Kundu, and P. Karpur, "Efficient use of Lamb waves for detecting defects in large plates," Ultrasonics **36**, 791–801 (1998).
[3]J. L. Rose, A. Pilarski, and J. J. Dirit, "An approach to guided wave mode selection for inspection of laminated plate," J. Reinf. Plastics Composites **12**, 536–544 (1993).
[4]N. Guo and P. Cawley, "The interaction of Lamb wave with delaminations in composite liminates," J. Acoust. Soc. Am. **94**, 2240–2246 (1993).
[5]S. H. D. Valdez and C. Soutis, "Real-time nondestructive evaluation of fiber composite laminates using low-frequency Lamb waves," J. Acoust. Soc. Am. **111**, 2026–2033 (2002).
[6]W. Lestari and P. Qiao, "Application of wave propagation analysis for damage identification in composite laminated beams," J. Compos. Mater. **39**, 1967–1984 (2005).
[7]M. Yang and P. Qiao, "Modeling and experimental detection of damage in various materials using the pulse-echo method and piezoelectric sensor/actuators," Smart Mater. Struct. **14**, 1083–1100 (2005).
[8]C. M. Yeum, H. Sohn, J. B. Ihn, and H. J. Lim, "Instantaneous delamination detection in a composite plate using a dual piezoelectric transducer network," Compos. Struct. **94**, 3490–3499 (2012).
[9]C-T. Ng and M. Veidt, "Scattering of the fundamental anti-symmetric Lamb wave at delaminations in composite laminates," J. Acoust. Soc. Am. **129**, 1288–1296 (2011).
[10]G. Petculescu, S. Krishaswamy, and J. D. Achenbach, "Group delay measurements using modally selective Lamb wave transducers for detection and sizing of delaminations in composites," Smart Mater. Struct. **17**, 015007 (2008).
[11]S. S. Kessler, S. M. Spearing, and C. Soutis, "Damage detection in composite materials using Lamb wave methods," Smart Mater. Struct. **11**, 269–278 (2002).
[12]C. Ramadas, K. Balasubramaniam, M. Joshi, and C. V. Krishnamurthy, "Interaction of the primary anti-symmetric Lamb mode (A_0) with symmetric delaminations: Numerical and experimental studies," Smart Mater. Struct. **18**, 085011 (2009).
[13]C. Ramadas, K. Balasubramaniam, M. Joshi, and C. V. Krishnamurthy, "Interaction of guided Lamb waves with an asymmetrically located delamination in a laminated composite plate," Smart Mater. Struct. **19**, 065009 (2010).
[14]T. Hayashi and K. Kawashima, "Multiple reflections of Lamb waves at a delamination," Ultrasonics **40**, 193–197 (2002).
[15]H. Sohn, D. Dutta, J. Y. Yang, H. J. Park, M. DeSimio, S. Olsen, and E. Swenson, "Delamination detection in composites through guided wave field image processing," Compos. Sci. Technol. **71**, 1250–1256 (2011).
[16]Y. Liu and J. E. Michaels, "A methodology for structural health monitoring with diffuse ultrasonic waves in the presence of temperature variations," Ultrasonics **43**, 717–731 (2005).
[17]T. Clarke, P. Cawley, P. D. Wilcox, and A. J. Croxford, "Evaluation of the damage detection capacity of a sparse-array guided-wave SHM system applied to a complex structure under varying thermal conditions," IEEE Trans. Ultrason. Ferroelectr. Freq. Control **56**, 2666–2678 (2009).
[18]C. K. Oh and H. Sohn, "Damage diagnosis under environmental and operational variations using unsupervised support vector machine," J. Sound Vib. **325**, 224–239 (2009).
[19]H. J. Lim, M. K. Kim, H. Sohn, and C. Y. Park, "Impedance based damage detection under varying temperature and loading conditions," NDT&E Int. **44**, 740–750 (2011).
[20]H. Sohn, G. Park, J. R. Wail, N. P. Limback, and C. R. Farrar, "Wavelet-based active sensing for delamination detection in composite structures," Smart Mater. Struct. **13**, 153–160 (2004).
[21]S. B. Kim and H. Sohn, "Instantaneous reference-free crack detection based on polarization characteristics of piezoelectric materials," Smart Mater. Struct. **16**, 2375–2387 (2007).
[22]H. W. Park, H. Sohn, K. H. Law, and C. R. Farrar, "Time reversal active sensing for health monitoring of a composite plate," J. Sound Vib. **302**, 50–66 (2007).
[23]S. G. Mallat and Z. Zhang, "Matching pursuits with time-frequency dictionaries," IEEE Trans. Sig. Process. **41**, 3397–3415 (1993).
[24]J. C. Hong, K. H. Sun, and Y. Y. Kim, "The matching pursuit approach based on the modulated Gaussian pulse for efficient guided-wave damage inspection," Smart Mater. Struct. **14**, 548–560 (2005).
[25]C. M. Yeum, H. Sohn, and J. B. Ihn, "Lamb wave mode decomposition using concentric ring and circular piezoelectric transducers," Wave Motion **48**, 358–370 (2011).
[26]C. H. Wang and L. R. F. Rose, "Wave reflection and transmission in beams containing delamination and inhomogeneity," J. Sound Vib. **264**, 851–872 (2003).
[27]M. Palacz, M. Krawczuk, and W. Ostachowicz, "The spectral finite element model for analysis of flexural-shear coupled wave propagation. Part 2: Delaminated multilayer composite beam," Compos. Struct. **68**, 45–51 (2005).
[28]D. E. Adams, *Health Monitoring of Structural Materials and Components* (John Wiley and Sons, West Sussex, UK, 2007), Chap. 3, pp. 113.
[29]S. Gopalakrishnan, "Modeling aspects in finite elements," in *Encyclopedia of Structural Health Monitoring* (John Wiley and Sons, West Sussex, UK, 2009), Vol. 2, Chap. 42, pp. 791–809.
[30]S. J. Lee and H. Sohn, "Active self-sensing scheme development for structural health monitoring," Smart Mater. Struct. **15**, 1734–1746 (2006).
[31]S. Quek, D. Almond, L. Nelson, and T. Barden, "A novel and robust thermal wave signal reconstruction technique for defect detection in lock-in thermography," Meas. Sci. Technol. **16**, 1223–1233 (2005).